

Echo Phenomena in Large Systems of Coupled Oscillators

Edward Ott, John H. Plutig, Thomas M. Antonsen and Michelle Girvan

University of Maryland, College Park, MD 20742

Abstract

As exemplified by the Kuramoto model, large systems of coupled oscillators may undergo a transition to phase coherence with increasing coupling strength. It is shown that below the critical coupling strength for this transition such systems may be expected to exhibit ‘echo’ phenomena: a stimulation by two successive pulses separated by a time interval τ leads to the spontaneous formation of response pulses at a time $\tau, 2\tau, 3\tau \dots$, after the second stimulus pulse. Analysis of this phenomenon, as well as illustrative numerical experiments, are presented. The theoretical significance and potential uses of echoes in such systems are discussed.

PACS numbers: 05.45.Xt, 05.45.-a, 89.75.-k

I. INTRODUCTION

Due to their occurrence in a wide variety of circumstances, systems consisting of a large number of coupled oscillators with different natural oscillation frequencies have been the subject of much scientific interest[1, 2]. Examples where the study of such systems is thought to be relevant are synchronous flashing of fireflies[3] and chirping of crickets[4], synchronous cardiac pacemaker cells[5], brain function[6], coordination of oscillatory neurons governing circadian rhythms in mammals[7], entrainment of coupled oscillatory chemically reacting cells[8], Josephson junction circuit arrays[9], etc. The globally-coupled, phase-oscillator model of Kuramoto[10, 11] exemplifies the key generic feature of large systems of coupled oscillators. In particular, Kuramoto considered the case where the distribution function of oscillator frequencies was monotonically decreasing away from its peak value, and he showed that, as the coupling strength K between the oscillators is increased through a critical coupling strength K_c , there is a transition to sustained global cooperative behavior. In this state ($K > K_c$) a suitable average over the oscillator population (this average is often called the ‘order parameter’) exhibits steady macroscopic oscillatory behavior. For $K < K_c$ a stimulus may transiently induce macroscopic oscillations, but the amplitude of these coherent oscillations (i.e., the magnitude of the order parameter) decays exponentially to zero with increasing time[11]. In the present paper we consider the Kuramoto model in the parameter range $K < K_c$, and we demonstrate that ‘echo’ phenomena occur for this system. The basic echo phenomenon can be described as follows: A first stimulus is applied at time $t = 0$, and the response to it dies away; next, a second stimulus is applied at a later time, $t = \tau$, and its response likewise dies away; then at time $t = 2\tau$ (also possibly at $n\tau$, for $n = 3, 4, \dots$) an echo response spontaneously builds up and then decays away. An illustrative example is shown in Fig. 1, which was obtained by numerical simulation (see Sec. IV for details). In order for this phenomenon to occur, the system must have two fundamental attributes, nonlinearity and memory. Nonlinearity is necessary because the sum of the responses to each of the individual stimulus pulses in the absence of the other pulse is simply the decay that occurs immediately after the individual stimuli, without the echo. Memory is necessary in the sense that the system state after the decay of the second pulse must somehow encode knowledge of the previous history even though the global average of the system state, as represented by the order parameter, is approximately the same as

before the two pulses were applied.

Echo phenomena of this type, occurring in systems of many oscillators having a spread in their natural oscillation frequencies, have been known for a long time. The first example was the ‘spin echo’ discovered in 1950 by Hahn[12], where the distribution of frequencies resulted from the position dependence of the precession frequency of nuclear magnetic dipoles in an inhomogeneous magnetic field. [The spin echo forms the basis for modern magnetic resonance imaging (MRI).] Subsequently, echoes for cyclotron orbits of charged particles in a magnetic field have been studied for the cases in which the distribution in frequency was due to magnetic field inhomogeneity[13], relativistic dependence of the particle mass on its energy[14], and Doppler shifts of the cyclotron frequency[15]. Another notable case is that of plasma waves, where the frequency distribution results from the Doppler shift of the wave frequency felt by charged particles with different streaming velocities[16]. Although echo phenomena are well-known in the above settings, they have so far not received attention in the context of the Kuramoto model and its many related situations. It is our purpose in the present paper to investigate that problem. Two possible motivations for our study of echoes in the Kuramoto model are that they provide increased basic understanding of the model and also that they may be of potential use as a basis for future diagnostic measurements of related systems (see Sec. V).

In what follows, Sec. II will give a formulation of the model problem that will be analyzed in Sec. III and numerically simulated in Sec. IV, while Sec. V will provide discussion of the implications of the results obtained.

II. FORMULATION

We consider the basic Kuramoto model supplemented by the addition of a δ -correlated noise term $n(t)$ and two impulsive stimuli, one at time $t = 0$, and the other at time $t = \tau$,

$$d\theta_i/dt = \omega_i + K/N \sum_{j=1}^N \sin(\theta_j - \theta_i) - h(\theta_i)\Delta(t) + n(t) , \quad (1)$$

$$\Delta(t) = \hat{d}_0\delta(t) + \hat{d}_1\delta(t - \tau) , \quad (2)$$

$$\langle n(t)n(t') \rangle = 2\xi\delta(t - t') , \quad (3)$$

$$h(\theta) = \sum_n h_n e^{in\theta} , \quad h_n = h_{-n}^* , \quad h_0 = 0 , \quad (4)$$

where h_{-n}^* denotes the complex conjugate of h_{-n} . In the above $\theta_i(t)$ represents the angular phase of oscillator i , where $i = 1, 2, \dots, N \gg 1$; and ω_i is the natural frequency of oscillator i where we take ω_i for different oscillators (i.e., different i) to be distributed according to some given, time-independent distribution function $g(\omega)$, where $g(\omega)$ has an average frequency $\bar{\omega} = \int \omega g(\omega) d\omega$, is symmetric about $\omega = \bar{\omega}$, and monotonically decreases as $|\omega - \bar{\omega}|$ increases.

To motivate the impulsive stimuli term, consider the example of a population of many fireflies, and imagine that the stimuli at $t = 0$ and at $t = \tau$ are external flashes of light at those times, where the constants \hat{d}_0 and \hat{d}_1 in Eq. (2) represent the intensity of these flashes. We hypothesize that a firefly will be induced by a stimulus flash to move its flashing phase toward synchronism with the stimulus flash. Thus a firefly that has just recently flashed will reset its phase by retarding it, while a firefly that was close to flashing will advance its phase. The amount of advance or retardation is determined by the ‘reset function’, $h(\theta)$. Since the reset function $h(\theta)$ depends on properties of the fireflies, we do not specify it further. Let θ_i^+ and θ_i^- represent the phases of oscillator i just after and just before a stimulus flash at $t = 0$ or $t = \tau$. Then we have from Eq. (1) that

$$\int_{\theta_i^-}^{\theta_i^+} \frac{d\theta}{h(\theta)} = \hat{d}_p; \quad p = 0, 1. \quad (5)$$

Letting $F(\theta) = \int^\theta d\theta/h(\theta)$, we obtain

$$\theta_i^+ = F^{-1}(\hat{d}_p + F(\theta_i^-)). \quad (6)$$

In our subsequent analysis in Sec. III, we will for convenience assume that \hat{d}_p is small, in which case $(\theta_i^+ - \theta_i^-)$ is small, and we can use the approximation,

$$\theta_i^+ \cong \theta_i^- + \hat{d}_p h(\theta_i^-); \quad p = 0, 1. \quad (7)$$

Following Kuramoto we introduce the complex valued order parameter $R(t)$,

$$R(t) = \frac{1}{N} \sum_{j=1}^N e^{i\theta_j(t)}, \quad (8)$$

in terms of which Eq. (1) can be rewritten as

$$d\theta_i/dt = \omega_i + (K/N) \text{Im}[e^{-i\theta_i} R(t)] - h(\theta_i)\Delta(t) + n(t). \quad (9)$$

In our analysis in Sec. III we will take the limit $N \rightarrow \infty$ useful for approximating the situation where $N \gg 1$. In that limit it is appropriate to describe the system state by a continuous distribution function $f(\theta, \omega, t)$, where

$$\int_0^{2\pi} f(\theta, \omega, t) \frac{d\theta}{2\pi} = 1, \quad (10)$$

and the fraction of oscillators with angles and natural frequencies in the ranges $(\theta, \theta + d\theta)$ and $(\omega, \omega + d\omega)$ is $f(\theta, \omega, t)g(\omega)d\omega d\theta/2\pi$. The conservation of the number of oscillators then gives the time evolution equation for $f(\theta, \omega, t)$,

$$\frac{\partial f}{\partial t} + \frac{\partial}{\partial \theta} \{f [\omega + K \text{Im}(R(t)e^{-i\theta}) - h(\theta)\Delta(t)]\} = \xi \frac{\partial^2 f}{\partial \theta^2}, \quad (11)$$

$$R^*(t) = \int d\omega f_1(\omega, t)g(\omega), \quad (12)$$

where we take $f(\omega, \theta, t) \equiv 1$ for $t < 0$, and, in writing Eq. (12), f_1 represents the $e^{i\theta}$ component of the Fourier expansion of $f(\omega, \theta, t)$ in θ ,

$$f(\omega, \theta, t) = \sum_{n=-\infty}^{+\infty} f_n(\omega, t)e^{in\theta}, \quad (13)$$

with $f_0 = 1$, $f_n = f_{-n}^*$. As seen in Eq. (11), the effect of the noise term in Eq. (1) is to introduce diffusion in the phase angle θ whose strength is characterized by the phase diffusion coefficient ξ .

In Sec. III we will solve Eqs. (11) and (12) for the case $d_p \ll 1$, thus demonstrating the echo phenomenon as described in Sec. I. In Sec. IV we will present numerical solutions of Eq. (1) for large N .

III. ANALYSIS

A. Amplitude expansion

In order to proceed analytically we use a small amplitude expansion and obtain results to second order (i.e., up to quadratic in the small amplitude). This will be sufficient to obtain the echo phenomenon. We introduce a formal expansion parameter ϵ , as follows,

$$f = 1 + \epsilon f^{(1)} + \epsilon^2 f^{(2)} + \mathcal{O}(\epsilon^3); \quad (14)$$

$\hat{d}_p = \epsilon d_p$ for $p = 0, 1$; $R = \epsilon R^{(1)} + \epsilon^2 R^{(2)} + \mathcal{O}(\epsilon^3)$; $R^{(m)*} = \int g f_1^{(m)} d\omega$; where $f^{(m)} = \sum_n f_n^{(m)} \exp(in\theta)$. (Although we formally take $\epsilon \ll 1$, when we finally get our answers, the results will apply for $\epsilon = 1$ and $d_p = \hat{d}_p$, if $\hat{d}_p \ll 1$.)

B. Order ϵ

In linear order (i.e., $\mathcal{O}(\epsilon)$) from Eq. (11) we have for the component of $f^{(1)}$ varying as $e^{i\theta}$,

$$\frac{\partial f_1^{(1)}}{\partial t} + (i\omega + \xi)f_1^{(1)} = \frac{K}{2}R^{(1)*} + ih_1\Delta(t), \quad R^{(1)*}(t) = \int f^{(1)}gd\omega, \quad (15)$$

where $f_1^{(1)}(\omega, t) = 0$ for $t < 0$ and $R^{(1)*}$ is the complex conjugate of $R^{(1)}$. Due to the delta function term on the right hand side of Eq. (15), $ih_1d_0\delta(t)$, at the instant just after the first delta function (denoted $t = 0^+$), $f_1^{(1)}$ jumps from zero just before the delta function (denoted $t = 0^-$) to the value $f_1^{(1)}(\omega, 0^+) = ih_1d_0$. Making use of this observation, in Appendix I we solve Eq. (15) for $0 < t < \tau$, with the result that, for $K < K_c$,

$$f_1^{(1)} = A(\omega)e^{-(i\omega+\xi)t} + \text{(a more rapidly exponentially decaying component)}, \quad (16)$$

where

$$A(\omega) = ih_1d_0/D[-(i\omega + \xi)], \quad (17)$$

$$D(s) = 1 - \frac{K}{2} \int_{-\infty}^{+\infty} \frac{g(\omega)d\omega}{s + \xi + i\omega}, \quad \text{for } Re(s) > 0, \quad (18)$$

and $D(s)$ for $Re(s) \leq 0$ is defined from Eq.(18) by analytic continuation. Since Eq. (16) applies for $0 < t < \tau$, we have that just before the application of the second delta function stimulus ($t = \tau^-$),

$$f_1^{(1)}(\omega, \tau^-) \cong A(\omega)e^{-(i\omega+\xi)\tau}, \quad (19)$$

where we have neglected the second term on the right hand side of Eq. (16) on the basis that, due to its more rapid exponential decay, it is small compared to the first term.

Roots of $D(s) = 0$ govern the stability of the state with $R^{(1)} = 0$. Let $s = s_0$ denote the root of $D(s) = 0$ with the largest real part. If $Re(s_0) < 0$ the state $R^{(1)} = 0$ is stable, and a perturbation away from $R^{(1)} = 0$ decays to zero with increasing t at the exponential rate $Re(s_0)$. If $Re(s_0) > 0$, then the perturbation grows and $R^{(1)}$ eventually saturates into a sustained nonlinear state of coherent cooperative oscillatory behavior[10, 11]. In general, $Re(s_0)$ is an increasing function of the coupling constant K , and $Re(s_0) \gtrless 0$ for $K \gtrless K_c$,

where K_c is a critical value that depends on ξ and $g(\omega)$. Throughout this paper we shall be considering only the case $K < K_c$ for which $Re(s_0) < 0$.

It is instructive to consider $\xi = 0$. In that case, the first term in Eq. (16) is of constant magnitude in time, but, as time t increases, it oscillates more and more rapidly as a function of ω . Because of this increasingly rapid variation in ω , the contribution of this term to $R^{(1)*}(t) = \int g f_1^{(1)} d\omega$ decays in time (see Appendix I), and it does so at the same time-asymptotic rate as the contribution from the second more rapidly exponentially decaying contribution in Eq. (16). Thus the order parameter magnitude decays away, but the distribution function $f_1^{(1)}$ can still have a component (the first term in Eq. (16)) due to the pulse that has not decayed away. A similar conclusion applies for $\xi > 0$ provided that ξ is substantially less than the damping for the second term in Eq. (16). This is the source of the ‘memory’ referred to in Sec. I. It is also worth noting that the first term in Eq. (16) can be thought of as the manifestation of the continuous spectrum of the Kuramoto problem, discussed in detail in Ref. [17]. Thus the echo phenomenon that we derive subsequently can be regarded as an observable macroscopic consequence of the continuous spectrum, where by ‘macroscopic’ we mean that the effect can be seen through monitoring of the order parameter without the necessity of other more detailed knowledge of the distribution function.

It is also of interest to consider $f_n^{(1)}$ for $n \geq 2$. From Eq. (11) we obtain for $|n| \geq 2$

$$\frac{\partial f_n^{(1)}}{\partial t} + (in\omega + n^2\xi)f_n^{(1)} = inh_n\Delta(t) , \quad (20)$$

which does not have any contribution from the order parameter, R . For $\tau > t > 0$, Eq. (20) yields

$$f_n^{(1)}(\omega, t) = inh_n d_0 \exp[-(in\omega + n^2\xi)t] , \quad (21)$$

for $0 < t < \tau$, which, similar to the first term on the right hand side of Eq. (16), also oscillates increasingly more rapidly with ω as t increases. At time $t = \tau^-$ Eq. (21) yields

$$f_n^{(1)}(\omega, \tau^-) = inh_n d_0 \exp[-(in\omega + n^2\xi)\tau] , \quad (22)$$

for $|n| \geq 2$.

C. Order ϵ^2

Now proceeding to $\mathcal{O}(\epsilon^2)$ and again taking the $e^{i\theta}$ component of Eq. (11), we have

$$\frac{\partial f_1^{(2)}}{\partial t} + (i\omega + \xi)f_1^{(2)} - \frac{1}{2}KR^{(2)*} = -i \left\{ \frac{K}{2i}f_2^{(1)}R^{(1)} - \Delta(t) \sum_{n=-\infty}^{+\infty} h_{-(n-1)}f_n^{(1)} \right\} \quad (23)$$

where $R^{(1,2)*}(t) = \int_{-\infty}^{+\infty} g(\omega)f_1^{(1,2)}(\omega, t)d\omega$. The above equation is linear in $f_1^{(2)}$ and is driven by several inhomogeneous terms appearing on the right hand side of Eq. (23) that are quadratic in first order quantities. Since we are interested in the components of $f_1^{(2)}$ that result in echoes, and since, by our previous discussion, we expect that the echoes depend on the presence of *both* stimulus delta functions (i.e., the delta function $\delta(t)$ of strength d_0 and the delta function $\delta(t - \tau)$ of strength d_1), we are interested in the component of $f_1^{(2)}$ that is proportional to the product d_0d_1 for $t > \tau$. We denote this component $f_{1,e}^{(2)}$, where the subscript e stands for ‘echo’. From Eq. (23) we see that for $t > \tau$, the $f_{1,e}^{(2)}$ component of $f_1^{(2)}$ satisfied the following initial value problem

$$\frac{\partial f_{1,e}^{(2)}}{\partial t} + (i\omega + \xi)f_{1,e}^{(2)} - \frac{1}{2}KR_e^{(2)*} = 0 , \quad (24)$$

$$f_{1,e}^{(2)}(\omega, \tau^+) = id_1 \sum_{n=-\infty}^{+\infty} h_{-(n-1)}f_n^{(1)}(\omega, \tau^-) , \quad (25)$$

$$R_e^{(2)*}(t) = \int_{-\infty}^{+\infty} g(\omega)f_{1,e}^{(2)}(\omega, t)d\omega . \quad (26)$$

Since $f_n^{(1)}(\omega, \tau^-)$ is proportional to d_0 (see Eqs. (19) and (22)), we see that the solution of Eqs. (24)–(26) for $f_{1,e}^{(2)}$ and $R_e^{(2)}$ will indeed be proportional to d_0d_1 as desired.

We solve Eqs. (24)–(26) by taking Laplace transforms,

$$\hat{f}_{1,e}^{(2)}(\omega, s) = \int_{\tau}^{\infty} e^{-st} f_{1,e}^{(2)}(\omega, t)dt , \quad (27)$$

$$\hat{R}_{e*}^{(2)}(s) \equiv \int_{\tau}^{\infty} e^{-st} R_e^{(2)*}(t)dt , \quad (28)$$

in terms of which we obtain from Eq. (24)

$$\hat{f}_{1,e}^{(2)} = \hat{R}_{e*}^{(2)} \frac{K/2}{s + \xi + i\omega} + \frac{f_{1,e}^{(2)}(\omega, \tau^+)e^{-s\tau}}{s + \xi + i\omega} . \quad (29)$$

Multiplying Eq. (29) by $g(\omega)d\omega$ and integrating from $\omega = -\infty$ to $\omega = +\infty$, then yields

$$\hat{R}_{e*}^{(2)}(s) = \frac{e^{-s\tau}}{D(s)} \int_{-\infty}^{+\infty} \frac{f_{1,e}^{(2)}(\omega, \tau^+)}{s + \xi + i\omega} g(\omega)d\omega . \quad (30)$$

To find $R_e^{(2)*}(t)$ we take the inverse Laplace transform,

$$R_e^{(2)*}(t) = \frac{1}{2\pi i} \int_{-i\infty+\eta}^{+i\infty+\eta} e^{st} \hat{R}_{e*}^{(2)}(s) ds, \eta > 0. \quad (31)$$

For the purposes of evaluating the integral (31), we recall that $D(s) = 0$ has roots whose real parts correspond to the exponential decay rate of a response to an initial stimulus toward the $R = 0$ state. Thus, as before in our discussion of the linear response (see Eq. (16)), any poles at the roots of $D(s) = 0$ give contributions that we assume decay substantially faster with increasing $t > \tau$ than the diffusion induced exponential decay rate ξ . Since we are interested in echoes that we will find occur for $t = 2\tau, 3\tau, \dots$, we neglect contributions to Eq. (31) from such poles. Thus it suffices to consider only the contribution to Eq. (31) from the pole at $s + \xi + i\omega = 0$. Hence Eqs. (30) and (31) yield

$$R_e^{(2)*}(t) \cong \int_{-\infty}^{+\infty} e^{-(i\omega+\xi)(t-\tau)} \frac{f_{1,e}^{(2)}(\omega, \tau^+)}{D[-(i\omega + \xi)]} g(\omega) d\omega. \quad (32)$$

D. Echoes

In order to see how Eq. (32) results in echoes, we recall our previous results, Eqs. (25), (19) and (21) for $f_{1,e}^{(2)}(\omega, \tau^+)$, and combine them to obtain

$$f_{1,e}^{(2)}(\omega, \tau^+) = d_0 d_1 h_2 h_1^* \frac{\exp(i\omega\tau - \xi\tau)}{D^*[-(i\omega + \xi)]} - d_0 d_1 \sum_{|n| \geq 2} n h_n h_{n-1}^* \exp[-(in\omega + n^2\xi)\tau], \quad (33)$$

where we have used $h_0 = 0$, $h_n = h_n^*$, $f_{-1}^{(1)} = f_1^{(1)*}$, and the first term on the right side of Eq. (33) corresponds to $n = -1$ in Eq. (25). Putting Eq. (33) into Eq. (32), we see that we have an integral of a sum over terms with exponential time variations of the form

$$\exp\{-i\omega[t - (1 - n)\tau]\} \exp\{-\xi[t + (n^2 - 1)\tau]\}. \quad (34)$$

Considering the first exponential in Eq. (34), we see that, for large values of $|t - (1 - n)\tau|$, there is rapid oscillation of the integrand with ω , and the integral can therefore be expected to be near zero. However, such rapid oscillation is absent near the times $t = (1 - n)\tau$, at which a large value of $R_e^{(2)*}$ will occur. Since $t > \tau$, the relevant times occur for $n < -1$; e.g., for $n = -1$, we get an echo at $t = 2\tau$; for $n = -2$, we get an echo at $t = 3\tau$; etc. Therefore, we henceforth replace the summation over $|n| \geq 2$ in Eq. (33) by a summation from $n = -\infty$ to $n = -2$.

E. Evaluation for Lorentzian frequency distribution functions

We now consider the case of a Lorentzian frequency distribution,

$$g(\omega) = g_L(\omega) \equiv \frac{1}{\pi} \frac{\Delta}{(\omega - \bar{\omega})^2 + \Delta^2} = \frac{1}{2\pi i} \left\{ \frac{1}{\omega - (\bar{\omega} + i\Delta)} - \frac{1}{\omega - (\bar{\omega} - i\Delta)} \right\}, \quad (35)$$

where the right-most expression for $g_L(\omega)$ makes clear that $g_L(\omega)$ results from the sum of two pole contributions, one at $\omega = \bar{\omega} + i\Delta$, and one at $\omega = \bar{\omega} - i\Delta$. The quantity $\bar{\omega}$ represents the average frequency of the distribution, while Δ represents the width of the distribution. Consideration of the Lorentzian will be particularly useful to us because the integral (32) can be explicitly evaluated, and also because our numerical experiments in Sec. IV will be for the case of a Lorentzian frequency distribution function.

As a first illustration we consider the $n = -1$ term which results in an echo at $t = 2\tau$. We first evaluate $D(s)$ by inserting the pole-form for $g_L(\omega)$ into Eq. (18) and closing the integration path with a large semicircle of radius approaching infinity. This yields a single residue contribution to $D(s)$,

$$D(s) = 1 - \frac{K}{2} [s + \xi + i(\bar{\omega} - i\Delta)]^{-1}. \quad (36)$$

Note that the root of $D(s) = 0$ occurs at

$$s = -i\omega - \left(\xi + \Delta - \frac{K}{2} \right). \quad (37)$$

According to our previous assumptions, we require $K < K_c \equiv 2(\Delta + \xi)$ so that the $R = 0$ state is stable, and $(\Delta - K/2)\tau - \xi\tau \gg 1$ so that we can neglect contributions from the pole at the root $D(s) = 0$ in our approximation of (31) by (32). Using Eq. (36) and the $n = -1$ contribution to $f_{1,e}^{(2)}$ (i.e., the first term in (33)) in Eq. (32) we obtain for the echo term at $t = 2\tau$ (denoted $R_{2\tau}^{(2)*}(\epsilon)$),

$$R_{2\tau}^{(2)*}(t) = 2ih_1^*h_2d_0d_1\Delta \int_{-\infty}^{+\infty} \frac{d\omega}{2\pi i} \cdot \frac{\exp[-i\omega(t - 2\tau) - \xi t]}{[(\omega - \bar{\omega}) - i(\Delta - \frac{K}{2})][(\omega - \bar{\omega}) + i(\Delta - \frac{K}{2})]}. \quad (38)$$

For $t > 2\tau$ ($t < 2\tau$) the integrand exponentially approaches zero as $Im(\omega) \rightarrow -\infty$ ($Im(\omega) \rightarrow +\infty$), and we can therefore close the integration path with a large semicircle in the lower half ω -plane (upper half ω -plane). Thus the integral (38) is evaluated from the pole enclosed by the resulting path [i.e., the pole $\omega = \omega_0 - i(\Delta - \frac{K}{2})$ for $t > 2\tau$, and the pole $\omega = \omega_0 + i(\Delta - \frac{K}{2})$ for $t < 2\tau$],

$$R_{2\tau}^{(2)*}(t) = \frac{h_1^*h_2d_0d_1\Delta}{\Delta - (K/2)} e^{-i\bar{\omega}(t-2\tau) - \xi t} e^{-(\Delta - \frac{K}{2})|t-2\tau|}. \quad (39)$$

From Eq. (39) we see that we obtain an echo that is approximately symmetric in shape about $t = 2\tau$ (i.e., the envelope $\exp[-(\Delta - K/2)|t - 2\tau|]$ for $\xi \ll (\Delta - \frac{1}{2}K)$).

We can similarly evaluate the contribution $R_{m\tau}^{(2)*}(t)$ of echoes at $t = m\tau$ for $m = 3, 4, \dots$. For example, the result for the echo at $t = 3\tau$ is

$$R_{3\tau}^{(2)*} = \frac{2h_2^* h_3 d_0 d_1 \Delta}{\Delta - (K/4)} e^{-\xi(3\tau+t)} e^{-i\bar{\omega}(t-3\tau)} E(t - 3\tau), \quad (40)$$

$$E(t - 3\tau) = \begin{cases} \exp[\Delta(t - 3\tau)], & \text{for } t < 3\tau, \\ \exp -[(\Delta - \frac{1}{2}K)(t - 3\tau)], & \text{for } t > 3\tau. \end{cases} \quad (41)$$

Thus, in the case $\xi = 0$, the shape of the pulse envelope $E(t - 3\tau)$ is asymmetric about $t = 3\tau$, increasing at a more rapid exponential rate (namely, Δ) as t increases toward 3τ , than the slower exponential rate of decrease (namely, $\Delta - (K/2)$) as t increases away from 3τ . This is in contrast to the symmetrically shaped envelope $\exp[-(\Delta - \frac{1}{2}K)|t - 2\tau|]$ for the echo at $t = 2\tau$.

In Appendix II we present an evaluation of $R_{2\tau}^{(2)*}(t)$ for the case of a Gaussian frequency distribution function,

$$g(\omega) = g_G(\omega) \equiv [2\pi\Delta^2]^{-1/2} \exp[-(\omega - \bar{\omega})^2/(2\Delta^2)].$$

F. The small coupling limit

We now consider a general frequency distribution function $g(\omega)$ but for the case where the coupling between oscillators is small. That is, $K \ll \Delta$, where Δ denotes the frequency width of $g(\omega)$ about its mean value $\omega = \bar{\omega}$. In this case a good approximation is provided by setting $K = 0$. Thus $D[-(i\omega + \xi)] \cong 1$ and Eq. (33) yields

$$f_{1,e}^{(2)}(\omega, \tau^+) = d_0 d_1 \sum_{n=1}^{\infty} n h_n^* h_{n+1} \exp[-(-in\omega + n^2\xi)\tau], \quad (42)$$

where we have replaced n by $-n$ and used $h_n = h_{-n}^*$. Inserting Eq. (42) into Eq. (32) we obtain

$$R_e^{(2)*}(t) = \sum_{n=2}^{\infty} (n-1) d_0 d_1 h_{n-1}^* h_n \tilde{g}(t - n\tau) e^{-[(n^2-1)\tau+t]\xi}, \quad (43)$$

where $\tilde{g}(t)$ is defined by

$$\tilde{g}(t) = \int_{-\infty}^{+\infty} d\omega e^{-i\omega t} g(\omega). \quad (44)$$

Thus, for $K \ll \Delta$, the shape of the echoes at $t = 2\tau, 3\tau, \dots$ is directly given by the Fourier transform (44) of the frequency distribution function $g(\omega)$.

IV. SIMULATIONS

We have performed direct numerical simulations of the system (1) with a Lorentzian oscillator distribution (see Eq. (35)), $\bar{\omega} = 0$, $\Delta = 1$ (corresponding to $K_c = 2$), $\hat{d}_0 = \hat{d}_1$, $K = 1$, $\tau = 50$, and $\xi = 0$. At $t = 0^-$ we initialize each phase θ_i for $i = 1, 2, \dots, N$ randomly and independently with a uniform distribution in the interval $(0, 2\pi)$. We then apply the mapping given by Eq. (7) with $\hat{d}_p = \hat{d}_0$ to each θ_i in order to simulate the effect of the delta function at $t = 0$. Next we integrate Eq. (1) for each $i = 1, 2, \dots, N$ forward in time to $t = \tau^-$, again apply the mapping Eq. (7) (but now with $\hat{d}_p = \hat{d}_1$), and we then continue the integration. At each time step we also calculate $R(t)$ using Eq. (8). Figure 2 shows results for $\hat{d}_0 = \hat{d}_1 = 1/4$, and

$$h(\theta) = \sin \theta + \sin 2\theta ,$$

for several different system sizes, $N = 10^6$, 10^5 , and 10^4 . Figure 2(a-c) shows $|R(t)|$ versus t for $0 \leq t \leq 125$. The responses to the delta functions at $t = 0$ and τ , as well as the echo at time $t = 2\tau$ are clearly illustrated. The effect of lower N is to increase the fluctuations making the echo somewhat less distinct. We do not see any echo at $t = 3\tau$. This is in agreement with Eq. (40), since $h_3 = 0$ for the $h(\theta)$ employed in these computations. Figure 3 shows a blow-up of the numerically computed echo around the time $t = 2\tau$ for $N = 10^6$, 10^5 , and 10^4 . Also, plotted in Fig. 3 as asterisks is the result from our theoretical calculation Eq. (39). Reasonable agreement between the theoretical and computed echo shapes is obtained, although the agreement is somewhat obscured by fluctuation effects at the smaller system sizes (N). While our choice $\hat{d}_0 = \hat{d}_1 = 1/4$ might be regarded as questionable for applicability of the small amplitude approximation ($\hat{d}_p \ll 1$, for $p = 0, 1$) employed by Eq. (7) and by our theory of Sec. III, we have nonetheless evidently obtained good agreement between the theory and numerical experiment. Figure 4 illustrates the effect of varying the driving amplitude for a network of size $N = 10^4$. For $\hat{d}_0 = \hat{d}_1 = 1/8$ (Fig. 4(a)) the echo is swamped by the noise and is not seen. For $\hat{d}_0 = \hat{d}_1 = 1/4$ (Fig. 4(b), same as 2(a)) the echo seems to have appeared, but because of the noise, this conclusion is somewhat questionable. Finally, at the larger driving of $\hat{d}_0 = \hat{d}_1 = 1/2$, the echo is clearly present.

Figures 5(a) and 5(b) show the effect of changing $h(\theta)$. In particular, Fig. 5(a) shows

numerical results for $\hat{d}_0 = \hat{d}_1 = 1/4$, $N = 10^5$, and $h(\theta) = \sin \theta$, with all other parameters the same as before. Since h_2 is now zero, Eq. (39) now predicts that there is no echo, in agreement with Fig. 5(a). Figure 5(b) shows numerical results for $\hat{d}_0 = \hat{d}_1 = 1/4$, $N = 10^5$, and

$$h(\theta) = \sin \theta + \sin 2\theta + \sin 3\theta,$$

with all other parameters the same as before. Since h_1 , h_2 and h_3 are all nonzero, Eqs. (39) and (40) now predict echoes at both $t \cong 2\tau$ and at $t \cong 3\tau$, and this is confirmed by Fig. 5(b). Finally, we note that similar numerical experiments to all of the above have been repeated using a Gaussian $g(\omega)$, and these yield similar results (not shown).

V. DISCUSSION

Echo phenomena as used for MRI provide a powerful medical diagnostic tool. Echoes in plasmas have also been used as a basis for measuring velocity space diffusion of plasma particles[18]. Thus it is of interest to consider whether there are potential diagnostic measurement uses of echoes in the context of situations that can be described by the Kuramoto model and its variants. For example, we note that the amplitude of the echo varies exponentially with ξ , providing a possible means of determining the phase diffusion coefficient ξ . For example, the amplitude of the echo at $t = 2\tau$ varies as $e^{-\xi\tau}$. Thus the log of the ratio of measurements of the echo amplitude using two different values of τ , divided by the difference in the τ values, provides a potential means of estimating ξ . Also, as indicated by Eq. (43), if one can lower the coupling K sufficiently, then echoes provide a potential way of determining the oscillator frequency distribution function $g(\omega)$. In particular, for low K the distribution $g(\omega)$ is directly given by the inverse Fourier transform of the echo profile. On the other hand, we have seen from the simulations in Sec. IV that finite N leads to noise-like behavior that may compromise such attempts. We also note that the Kuramoto model is an idealization, and application to any given situation may require modifications of the model and theory to more closely correspond to the situation at hand. We, nevertheless, feel that consideration of echoes for diagnostics may be of potential use.

Furthermore, these phenomena are of theoretical interest from at least two points of view. First, as mentioned in Sec. IIIb, the memory required by the echo phenomenon can be thought of as leading to a macroscopically observable consequence of the continuous

spectrum[17] of the Kuramoto model. A second point of theoretical interest relates to the recent work in Ref. [19]. In that paper it was shown for a general class of initial conditions that are on a certain manifold of the infinite dimensional state space of the Kuramoto system, that the future time evolution of the order parameter is determined by the current value of the order parameter. In particular, there is an ordinary differential equation describing the order parameter evolution. The echo phenomenon provides an example showing that, if initial conditions do not lie on the specified manifold of Ref. [19], other behavior can occur. In particular, well after the second stimulus (at $t = \tau$) and well before the occurrence of the first echo (at $t = 2\tau$), the order parameter is essentially zero, yet it does not remain zero as would be predicted for initial conditions on the manifold of Ref.[19] for $K < K_c$. This is discussed further in Appendix III.

In conclusion, we hope that our work will stimulate experimental groups to investigate the type of situations we have addressed.

This work was supported by ONR (N00014-07-1-0734) and NSF (PHY0456249).

Appendix I: Linear Analysis

In this Appendix we solve Eq. (15) for $0 < t < \tau$ to obtain the solution (16) and (17) for $K < K_c$. Taking the Laplace transform, $\hat{u}(s) = \int_0^\infty u(t)e^{-st}dt$, Eq. (15) yields

$$\hat{f}_1^{(1)}(\omega, s) = \left(\frac{K}{2} \hat{R}_*^{(1)}(s) + ih_1 d_0 \right) / (s + \xi + i\omega) \quad (45)$$

where $\hat{R}_*^{(1)}(s)$ denotes the Laplace transform of $R^{(1)*}(t)$. Multiplying Eq. (45) by $g(\omega)d\omega$ and integrating from $\omega = -\infty$ to $\omega = +\infty$, we obtain

$$\hat{R}_*^{(1)}(s) = ih_1 d_0 I(s) / D(s) , \quad (46)$$

where $I(s) = \int_{-\infty}^{+\infty} d\omega g(\omega) / (s + \xi + i\omega)$ and $D(s) = 1 - (K/2)I(s)$. Inserting Eq. (46) in (45) gives

$$\hat{f}_1^{(1)}(\omega, s) = ih_1 d_0 [D(s)(s + \xi + i\omega)]^{-1} . \quad (47)$$

As noted in Sec. IIIb, $\hat{f}_1^{(1)}(\omega, s)$ has poles in s at the zeros of $D(s)$ and at $s = -(i\omega + \xi)$. These yield time dependences of the inverse Laplace transform of $\hat{f}_1^{(1)}$ (see Eq. (27)) that vary as $e^{s_0 t}$ and as $e^{-(i\omega + \xi)t}$, respectively, where s_0 denotes the root of $D(s) = 0$ with the least negative real part. For $t \approx \tau$ and $-[Re(s_0) + \xi]\tau \gg 1$, we can neglect the contributions

from poles arising from roots of $D(s) = 0$, and use only the contribution from the pole at $s = -(i\omega + \xi)$. From Eqs. (27) and (47) this yields

$$f_1^{(1)}(\omega, t) \cong ih_1 d_0 e^{-(i\omega + \xi)t} / D[-(i\omega + \xi)] , \quad (48)$$

thus confirming Eqs. (16) and (17).

Appendix II: Echo at $t = 2\tau$ for Gaussian $g(\omega)$

We consider the case $g(\omega) = g_G(\omega) \equiv (2\pi\Delta^2)^{-1/2} \exp[-(\omega - \bar{\omega})^2 / (2\Delta^2)]$. Putting this expression for $g(\omega)$ and the $n = -1$ contribution to $f_{1,e}^{(2)}$ (i.e., the first term in Eq. (33)) into Eq. (32) we have,

$$R_{2\tau}^{(2)*}(t) = \frac{h_1 h_2 d_0 d_1}{\sqrt{2\pi\Delta^2}} \int_{-\infty}^{+\infty} d\omega \frac{\exp - \left\{ \frac{[(\omega - \bar{\omega}) + i\Delta^2(t - 2\tau)]^2}{2\Delta^2} + \frac{\Delta^2}{2}(t - 2\tau)^2 + i\bar{\omega}(t - 2\tau) - \xi t \right\}}{D[-(i\omega + \xi)] D^*[-(i\omega + \xi)]} . \quad (49)$$

The collective damping rate is determined by the root of $D(s) = 0$ with the least negative real part. Denote this root $s = s_0$ where

$$s_0 = -(i\bar{\omega} + \xi + \gamma_0) = -(i\omega_0 + \xi) , \quad \omega_0 = \bar{\omega} - i\gamma_0 , \quad (50)$$

where $\gamma_0 > 0$ is real. Letting $F(\omega) \equiv D[-(i\omega + \xi)]$, continuing this function from real ω into the complex ω -plane, and expanding around $\omega = \omega_0$, we have

$$F(\omega) = (\omega - \omega_0)\eta + \mathcal{O}[(\omega - \omega_0)^2] , \quad (51)$$

where η is a complex constant. Letting $F_*(\omega)$ denote the continuation of the function of the real variable ω in Eq. (49), $D^*[-(i\omega + \xi)]$, into the complex ω -plane, we have that this function has a zero at $\omega = \omega_0^*$,

$$F_*(\omega) = (\omega - \omega_0^*)\eta^* + \mathcal{O}[(\omega - \omega_0^*)^2] . \quad (52)$$

Considering the oscillatory ω variation in the numerator of the integrand of Eq. (49) to be rapid (valid for $K \ll \gamma_0$), we can approximate the integral by the saddle point method, where the saddle point is at

$$\omega_{sp} = \bar{\omega} - i\Delta^2(t - 2\tau) ,$$

and the steepest descent path through $\omega = \omega_{sp}$ runs along the horizontal line $Im(\omega) = -\Delta^2(t - 2\tau)$ from $Re(\omega) = -\infty$ to $Re(\omega) = +\infty$ (see Fig. 6). From Fig. 6(a) we see that for

$\Delta^2|t - 2\tau| < \gamma_0$, the poles at $\omega = \bar{\omega} \pm i\gamma_0$ are not intercepted by the steepest descent path, while for $\Delta^2|t - 2\tau| > \gamma_0$ one of the poles is intercepted (e.g., Fig. 6(b)). In the case where a pole is intercepted, its contribution dominates the contribution from the saddle point by virtue of its time dependence, $e^{-\gamma_0|t-2\tau|}$, as opposed to the saddle point contribution time dependence, $e^{-\frac{1}{2}\Delta^2(t-2\tau)^2}$. Thus we obtain

$$R_{2\tau}^{(2)*}(t) \sim e^{-i\bar{\omega}(t-2\tau)-\xi t} \times \begin{cases} e^{-\frac{\Delta^2}{2}(t-2\tau)^2} & \text{for } |t - 2\tau| < 2\gamma_0/\Delta^2, \\ e^{-\gamma_0|t-2\tau|} & \text{for } |t - 2\tau| > 2\gamma_0/\Delta^2. \end{cases} \quad (53)$$

Near $\gamma_0 = \Delta^2|t-2\tau|/2$, the pole is near the saddle point, and a uniform asymptotic expansion of the integral (49) is necessary to obtain the transition between the two forms in Eq. (53).

Appendix III: Further Discussion of Ref.[19]

In Ref. [19], a broad class of noiseless (e.g., $\xi = 0$ in Eqs. (3) and (11)) globally coupled systems of phase oscillators was studied. The simplest example of this class is the Kuramoto model. Reference [19] considered Lorentzian $g(\omega)$ and a special class of initial conditions. Referring to Eq. (12), these initial conditions are of the form,

$$f_n(\omega, 0) = \alpha^n(\omega), \quad \text{for } n \geq 0, \quad (54)$$

and $f_n(\omega, 0) = f_{-n}^*(\omega, 0)$, for $n \leq 0$, where $|\alpha(\omega)| < 1$ for ω on the real axis, $\alpha(\omega)$ is analytic in $\text{Im}(\omega) < 0$, and $|\alpha(\omega)| \rightarrow 0$ as $\text{Im}(\omega) \rightarrow -\infty$. Under these conditions, Ref. [19] shows that the order parameters (or parameter), see Eq. (12), that describe the nonlinear, macroscopic time evolution of the given system satisfy a finite set of ordinary differential equations in time. Thus the order parameter dynamics is low dimensional, while the dynamics of the full system determining the evolution of the distribution function $f(\omega, \theta, t)$ is infinite dimensional[19]. For example, for the Kuramoto problem with the above conditions satisfied, Ref. [19] shows that

$$dR/dt + \left(\Delta - \frac{1}{2}K \right) R + \frac{1}{2}K\Delta|R|^2R = 0, \quad (55)$$

where we have taken $\bar{\omega} = 0$ in Eq. (35).

A consequence of Eq. (55) is that for $K < 2\Delta \equiv K_c$, $|R(t)|$ decreases monotonically to zero. This behavior is not followed in the echo phenomena we discuss in the present paper.

In particular, in Fig. 1, $|R(t)|$ is small between $t = \tau$ and $t = 2\tau$, but then *increased* to form the echo in the vicinity of time $t = 2\tau$. Referring to Eq. (34) and our subsequent discussion, we see that this is because there is a component of $f_1(\omega, t)$ that varies as $\exp[-i\omega(t - 2\tau)]$. Identifying $f_1(\omega, 0)$ in the linear problem with $\alpha(\omega)$ in the nonlinear problem [Eq. (54)] and considering t_0 as a new initial time (shift time so that t_0 goes to $t = 0$), we see that $\alpha(\omega) \sim \exp[-i\omega(t_0 - 2\tau)]$. If we take t_0 to be such that $\tau < t_0 < 2\tau$ and $|R(t_0)|$ is small, then $\alpha(\omega)$ does not satisfy the condition of Ref. [19] that $\alpha(\omega) \rightarrow 0$ as $\text{Im}(\omega) \rightarrow -\infty$. However, if $t_0 > 2\tau$, then it does. Thus the increase of $|R(t)|$ occurs only when the hypothesis under which Eq. (55) was derived does not hold.

More generally, consider an initial condition for the original Kuramoto problem (without stimuli or noise) where $f_1(\omega, 0)$ is analytic on the real ω -axis. Expressing $f_1(\omega, 0)$ as a Fourier integral transform, we have

$$f_1(\omega, 0) = \int_{-\infty}^{+\infty} e^{i\omega\eta} k(\eta) d\eta, \quad (56)$$

where $k(\eta)$ is the Fourier transform of $f_1(\omega, 0)$. Since $f_1(\omega, 0)$ is analytic in ω , $k(\eta)$ decreases exponentially for sufficiently large η ,

$$|k(\eta)| < H e^{-\beta\eta}, \quad \text{if } \eta > \eta_0, \quad (57)$$

for some set of positive constants H, β, η_0 . Using the Laplace transform technique (as in Appendix I), it can be shown that the solution to the linearized initial value Kuramoto problem contains a component of $f_1(\omega, t)$ of the form $\exp(-i\omega t) f_1(\omega, 0)$, which we can express using Eq. (56) as

$$\exp(-i\omega t) f_1(\omega, 0) = \int_{-\infty}^t e^{-i\omega(t-\eta)} k(\eta) d\eta + \int_t^{\infty} e^{i\omega(\eta-t)} k(\eta) d\eta. \quad (58)$$

Setting $t = t_0$ and regarding $t = t_0$ as a new initial condition time, we note that the initial condition consists of two terms, namely the first and second integrals on the right hand side of Eq. (58). For $t_0 > \eta_0$ sufficiently large, the second integral is smaller than the first by a factor of order $\exp(-\beta t_0)$. Furthermore, the first integral satisfies the condition $f_1(\omega, t_0) \rightarrow 0$ as $\text{Im}(\omega) \rightarrow -\infty$ [because $(\eta - t_0) > 0$ for the first integral], while the second integral does not. Thus, if we choose to shift what we designate as the initial time to sufficiently large t_0 , then aside from an exponentially small component of order $\exp(-\beta t_0)$, the initial condition obeys the requirement of Ref. [19] that $f_1(\omega, t_0)$ goes to zero as $\text{Im}(\omega) \rightarrow -\infty$.

-
- [1] A. Pikovsky, M. Rosenblum and J. Kurths, *Synchronization: A Universal Concept in Nonlinear Science* (Cambridge University Press, 2001).
- [2] S. H. Strogatz, *Sync: The Emerging Science of Spontaneous Order* (Penguin Science Press, 2004).
- [3] J. Buck, Q. Rev. Biology **63**, 265 (1988).
- [4] T. J. Walker, Science **166**, 891 (1969).
- [5] D. C. Michaels, Circulation Research **61**, 704 (1987).
- [6] W. Singer, Ann. Rev. Physiology **55**, 349 (1993); R. Eckhorn et al., Biological Cybernetics **60**, 121 (1988); C. M. Gray, Nature **338**, 334 (1989).
- [7] S. Yamaguchi et al., Science **302**, 1408 (2002); T. M. Antonsen et al., arXiv:0711.4135.
- [8] I. Z. Kiss, Y. Zhai and J. L. Hudson, Science **296**, 1676 (2005).
- [9] K. Wiesenfeld and J. W. Swift, Phys. Rev. E **51**, 1020 (1995).
- [10] Y. Kuramoto, *Chemical Oscillations, Waves and Turbulence* (Springer, 1984); and in *International Symposium on Mathematical Problems in Theoretical Physics*, **39**, edited by H. Araki (Springer-Verlag, Berlin, 1975).
- [11] For reviews of the Kuramoto model see J. A. Acebron, et al., Rev. Mod. Phys. **77**, 137 (2005); S. H. Strogatz, Physica D **143**, 1 (2000); and E. Ott, *Chaos in Dynamical Systems*, second edition, chapter 6, section 6. (Cambridge University Press, 2002).
- [12] E. L. Hahn, Phys. Rev. **80**, 580 (1950).
- [13] R. W. Gould, Phys. Lett. **19**, 477 (1965); F. W. Crawford and R. S. Harp, J. Appl. Phys. **37**, 4405 (1966).
- [14] E. Ott, J. Plasma Phys. **4**, 471 (1970).
- [15] M. Porkolab and J. Sinnis, Phys. Rev. Lett. **21**, 1227 (1968).
- [16] T. M. O’Neil and R. W. Gould, Phys. Fluids **11**, 134 (1968); J. H. Malmberg, C. B. Wharton, R. W. Gould and T. M. O’Neil, Phys. Fluids **11**, 1147 (1968).
- [17] S. H. Strogatz, R. E. Mirollo and P. C. Matthews, Phys. Rev. Lett. **68**, 2730 (1992).
- [18] T. H. Jensen, J. H. Malmberg and T. M. O’Neil, Phys. Fluids **12**, 1728 (1969); C. H. Su and C. Oberman, Phys. Rev. Lett. **20**, 427 (1968); T. M. O’Neil, Phys. Fluids **11**, 2420 (1968).
- [19] E. Ott and T. M. Antonsen, Phys. Rev. Lett. (submitted).

Figure Captions

- Figure 1:** *Illustration of the echo phenomenon. Stimuli at times $t = 0$ and $t = \tau$ lead to direct system responses which rapidly decay away followed by an echo response at times 2τ . The ‘response’ plotted on the vertical axis is the magnitude of the complex valued order parameter, Eq. (8). See Sec. IV for details of this computation. The parameters used are the same as for Fig. 5(b) except that $N = 10^6$.*
- Figure 2:** *$|R(t)|$ versus t for (a) $N = 10^4$, (b) $N = 10^5$, and (c) $N = 10^6$, showing the echo at $t \cong 2\tau$ and the increase of fluctuations at lower N .*
- Figure 3:** *$|R(t)|$ versus t from Fig. 2 blown up around $t \cong 2\tau = 100$, for $N = 10^6$, 10^5 , 10^4 (solid curves) showing the increase of fluctuations at lower N . The asterisks are from the theoretical result from Eq. (39).*
- Figure 4:** *Simulations of 10^5 oscillators showing the effect of varying the size of the driving stimuli: (a) $\hat{d}_0 = \hat{d}_1 = 1/8$, (b) $\hat{d}_0 = \hat{d}_1 = 1/4$ (same as Fig. 2(a)), and (c) $\hat{d}_0 = \hat{d}_1 = 1/2$.*
- Figure 5:** *(a) Simulation of 10^5 oscillators for $\hat{d}_0 = \hat{d}_1 = 1/4$, $h(\theta) = \sin \theta$. In this case, no echoes at $t = 2\tau = 100$ and at $t = 3\tau = 150$ are observed. (b) Simulation of 10^5 oscillators for $\hat{d}_0 = \hat{d}_1 = 1/4$, and $h(\theta) = \sin \theta + \sin 2\theta + \sin 3\theta$. In this case, echoes are seen at $t = 2\tau = 100$ and at $t = 3\tau = 150$.*
- Figure 6:** *(a) Steepest descent path (dashed) through the saddle point $\omega = \omega_{sp}$ for $\Delta^2|t - 2\tau| < \gamma_0$. (b) The steepest descent path (dashed) for $\Delta^2(t - 2\tau) < -\gamma_0$. The dominant poles at the roots of $F(\omega) = 0$ and $F_*(\omega) = 0$ are shown as crosses, where in (b) the steepest descent path has intercepted the pole $\omega = \omega_0$ resulting in a pole contribution to $R_{2\tau}^{(2)*}(t)$.*

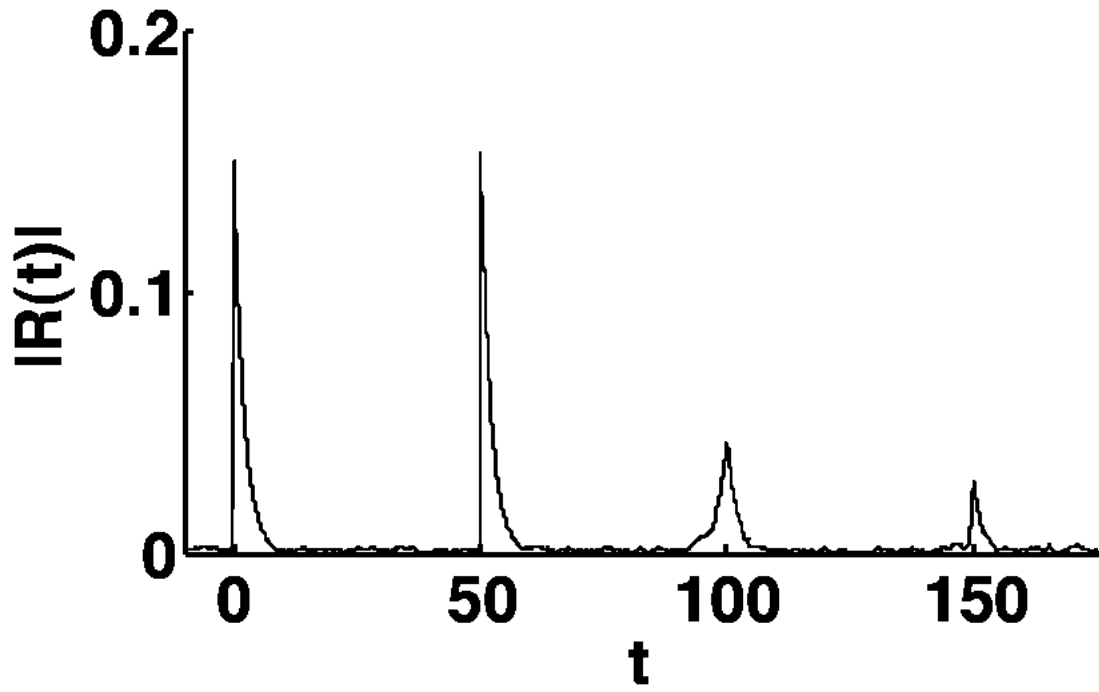


Figure 1

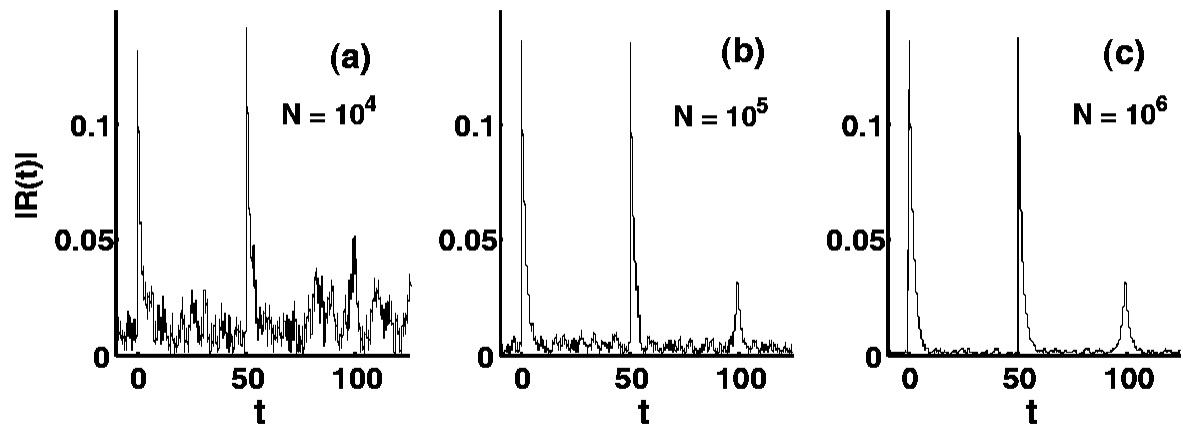


Figure 2

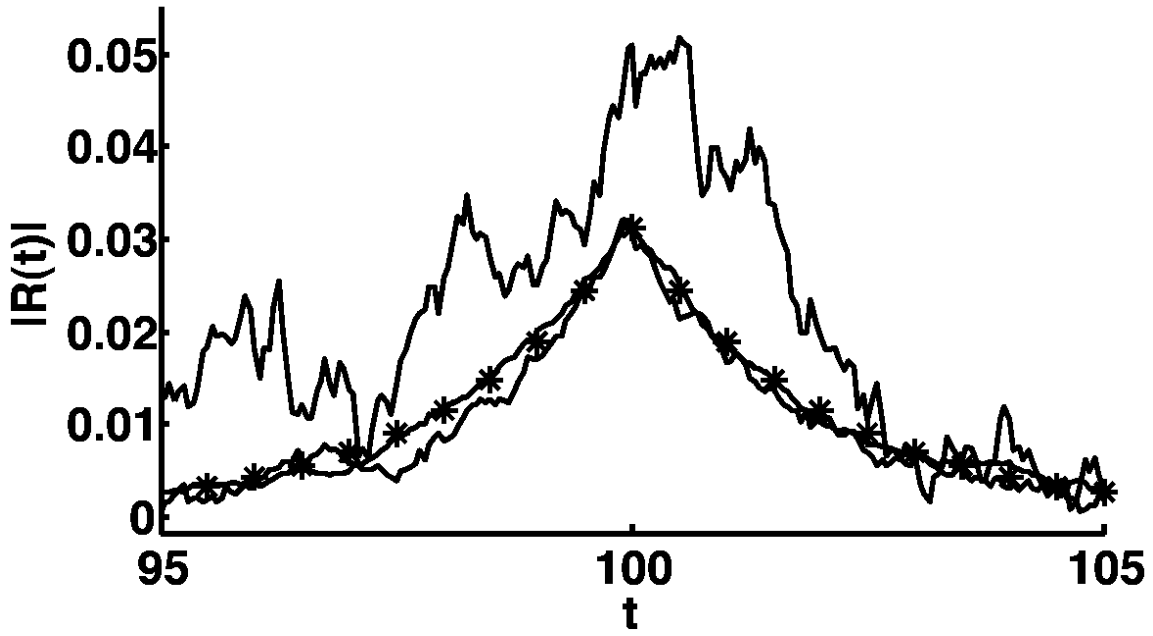


Figure 3:

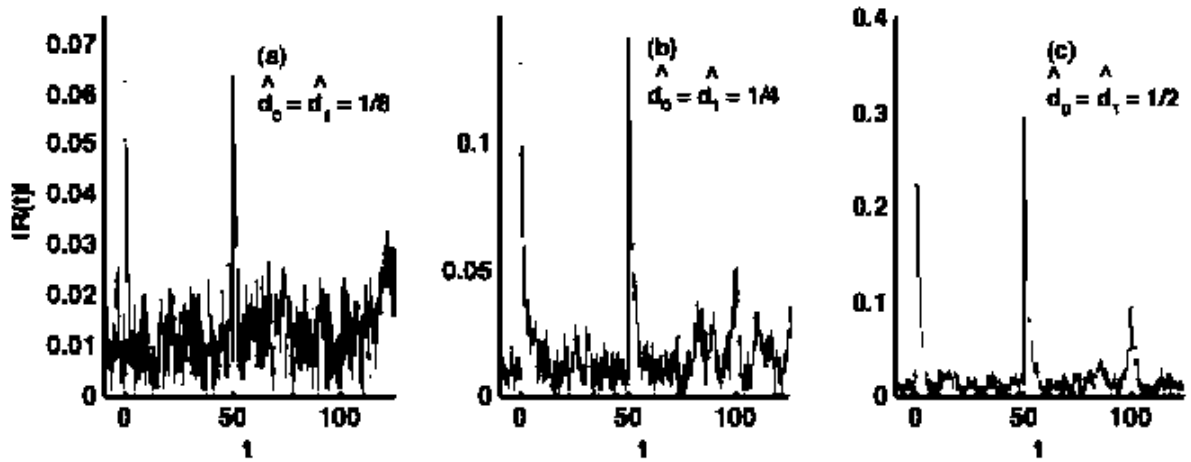


Figure 4

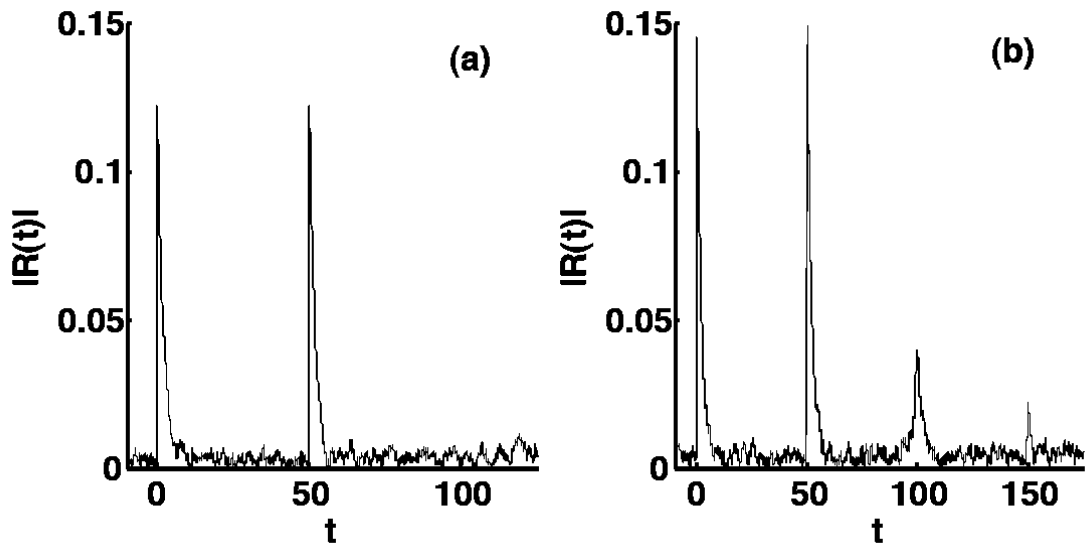


Figure 5:

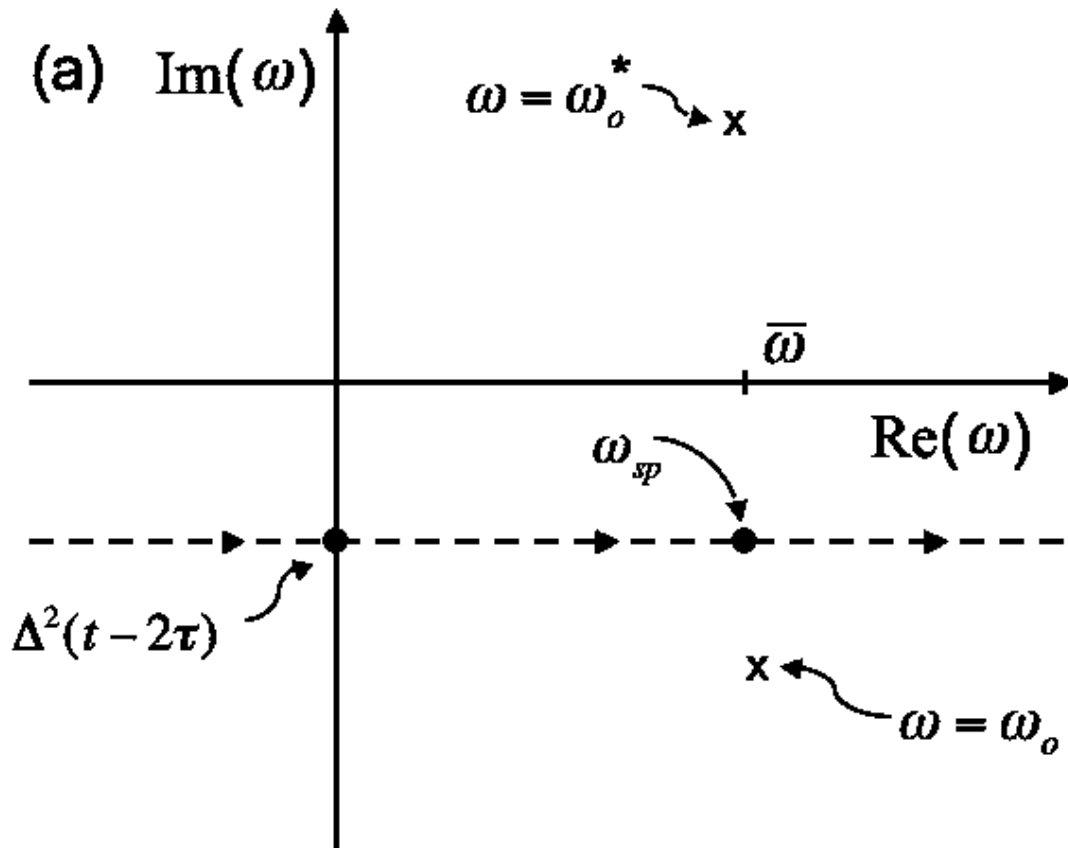


Figure 6a:

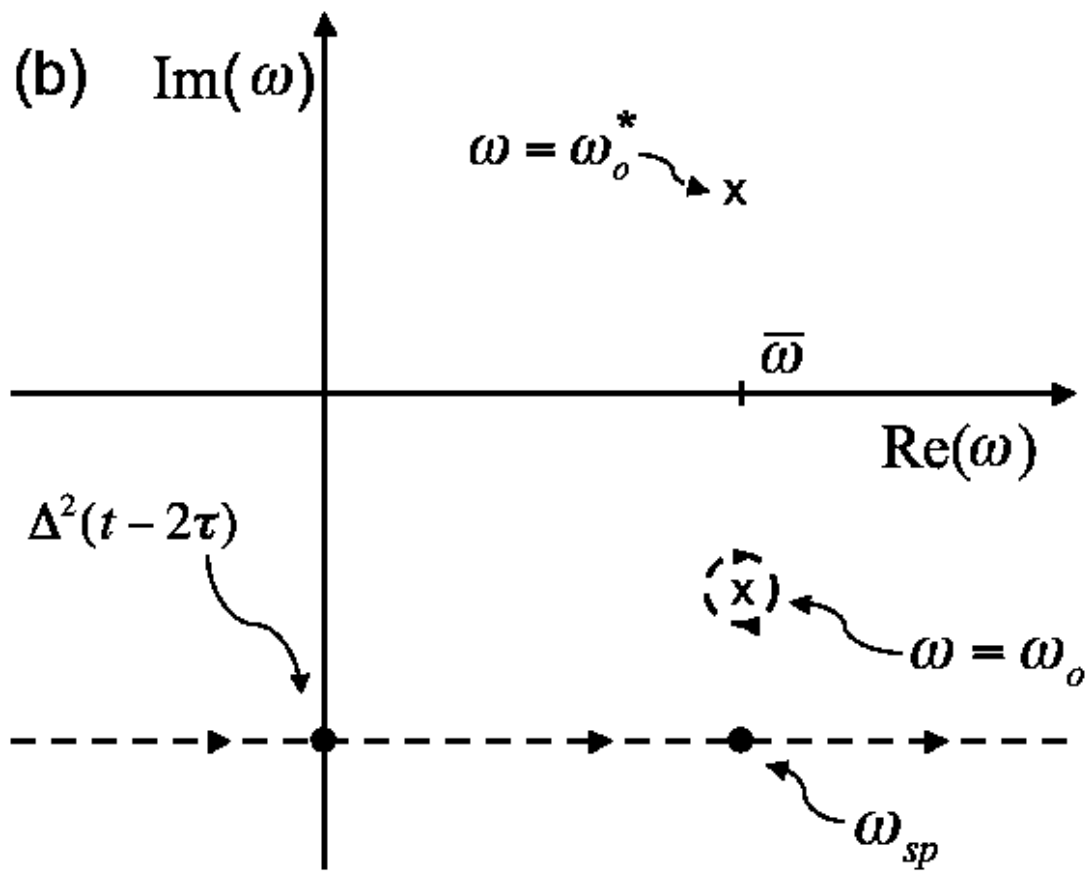


Figure 6b: